Radiative Divertor Plasma Behavior in L- and H-Mode Discharges with Argon Injection in

EAST

Radiative Divertor Plasma Behavior in L- and H-Mode Discharges with Argon Injection in EAST*

WANG Dongsheng (王东升)[1], GUO Houyang (郭后扬)[2,3], SHANG Yizi (尚毅梓)[4],
GAN Kaifu (甘开福)[2], WANG Huiqian (汪惠乾)[2], CHEN Yingjie (陈颖杰)[2],
LIU Shaocheng (刘少承)[2], WANG Liang (王亮)[2], GAO Wei (高伟)[2],
XIANG Lingyan (向玲燕)[2], WU Zhenwei (吴振伟)[2], LUO Guangnan (罗广南)[1,2],
and the EAST team

[1]Department of Modern Physics, University of Science and Technology of China,
 Hefei 230026, China
[2]Institute of Plasma Physics, Chinese Academy of Sciences, Hefei 230031, China
[3]Tri Alpha Energy, Inc., Rancho Santa Margarita, CA 92688-7010, USA
[4]School of Engineering and Applied Science, Harvard University, Boston 02138, USA

Abstract Introducing strong radiative impurities into divertor plasmas has been considered as an important way to mitigate the peak heat load at the divertor target plate for ITER, and will be employed in EAST for high power long pulse operations. To this end, radiative divertor experiments were explored under both low (L) and high (H) - mode confinement regimes, for the first time in EAST, with the injection of argon and its mixture (25% Ar in D_2). The Ar injection greatly reduced particle and heat fluxes to the divertor in L-mode discharges, achieving nearly complete detached divertor plasma regimes for both single null (SN) and double null (DN) configurations, without increasing the core impurity content. In particular, the peak heat flux was reduced by a factor of ~ 6, significantly reducing the intrinsic in-out divertor asymmetry for DN, as seen by both the new infra-red camera and the Langmuir probes at the divertor target. Promising results have also been obtained in the H-modes with argon seeding, demonstrating a significant increase in the frequency and decrease in the amplitude of the edge localized modes (ELMs), thus reducing both particle and heat loads caused by the ELMs. This will be further explored in the next experimental campaign with increasing heating power for long pulse operations.

Keywords: radiative divertor, impurity, heat flux, single null, double null

PACS: 52.55.Fa, 52.40.Hf, 52.25.Vy

DOI: 10.1088/1009-0630/15/7/02

1 Introduction

How to reduce the heat load to the divertor targets presents a major problem for highly powered tokamaks, which is also one of the most critical issues to be solved for ITER [1]. Several ways have been suggested for reducing heat loading on the divertor target, such as broadening the scrape-off layer or external gas (e.g., cold deuterium or impurity) injection into the divertor chamber near the strike point [2]. In particular, the radiative divertor technique has proven to be an effective method for reducing the target heat load by enhancing radiation losses induced by puffing deuterium (i.e., the plasma species itself) or by seeding the divertor with additional impurities, hence reducing the peak heat flux values to more tolerable levels before the plasma reaches the divertor targets. Another important benefit of radiative cooling in the divertor is the reduction of plasma temperature and sheath potential

at divertor targets, thereby lowering the ion impact energy. Radiative divertor experiments have been investigated on many tokamaks such as JET [3], DIII-D [4], ASDEX Upgrade [5], JT-60U [6], Alcator C-MOD [7], and HL-2A [8].

The Experimental Advanced Superconducting Tokamak (EAST) is the first fully superconducting tokamak, allowing both single null and double null divertor operations [9,10]. Its mission is to operate with high power and long pulses for investigating reactor-relevant issues under steady-state conditions. EAST was upgraded to a full graphite wall in the spring of 2008, with its maximum power handling capability presently being limited to ~ 2 MW/m². Therefore, additional radiation losses are required to decrease the power flow to the divertor target plate. In the near future, the divertor plasma facing materials and components (PFMC) will be changed into tungsten with a maximum power load of ~ 10 MW/m² to facilitate high power, long pulse op-

erations. Previous divertor experiments with deuterium and argon injection to actively control the divertor heat flux and improve the in-out asymmetry were carried out on EAST in Ohmic discharges [11,12]. Recently, radiative divertor experiments have also been performed in EAST under both low and high confinement regimes, i.e., L- and H-modes, with argon injection using the divertor gas injection system. A newly developed divertor infra-red (IR) camera system has been used to assess the target heat load, and comparisons have been made by using Langmuir probes measurements.

In this paper we will report these new results. The remainder of this paper is organized as follows. The experimental set-up is described in section 2. Section 3 summarizes key experimental results and discussions. Summary and conclusions are given in section 4.

2 Experimental setup

EAST has the capability to produce an ITER-relevant SN divertor configuration as well as a DN divertor configuration. Table 1 lists the major parameters of the two divertor configurations. Both SN and DN plasmas are conducted in a normal toroidal field with the $\mathbf{B} \times \nabla \mathbf{B}$-ion drift directed towards the lower divertor.

Table 1. Major parameters of EAST divertor configurations for single null (Shot 36736) and double null (Shot 31601)

Quantity	SN	DN
Major radius, R (m)	1.863	1.857
Minor radius, a (m)	0.452	0.453
Elongation at separatrix, κ_x	1.718	1.717
Upper triangularity at separatrix, δ_u	0.330	0.540
Lower triangularity at separatrix, δ_l	0.552	0.552
X-point height from the top of dome (m)	0.09	0.15
Connection length, L (m)	21.4	15.3
Cross-section area, (m^2)	1.004	0.974
Plasma volume, V_p (m^3)	11.5	11.1

EAST is equipped with a flexible, multi-purpose gas-puffing system, as shown in Fig. 1. With this new gas puffing system, we have injected deuterium and high-Z impurity (argon) into the divertor plasma to reduce the heat flux at the divertor target plate and control in-out asymmetry. Argon (Ar) is selected for the seeded impurity because it radiates effectively at the temperatures prevailing in the divertor. In addition, Ar also has a relatively short ionization mean-free path, making argon neutral less likely to leak from the divertor into the main chamber [13]. Since the first wall and divertor armors are graphite, carbon is presently the dominant intrinsic impurity in EAST. A new cryopump has been installed under the lower outer divertor target, which is an important component of modern tokamaks to exhaust neutrals and impurities. The experiments were

primarily focused on L-mode discharges heated by the lower hybrid wave, but Ar seeding into H-mode plasma was also tried on EAST. Ar was injected from the outer target strike point with the ion grad-B drift towards the lower divertor in SN and DN divertor configurations, with simultaneous divertor pumping. The major parameters for the two divertor configurations are listed in Table 1. Typical discharge parameters for the L-mode plasmas are: I_p=400∼600 kA, B_T=2 T, line-averaged density $\bar{n}_e = 1.0 \sim 5.0 \times 10^{19}$ m^{-3}. To quantify the degree of magnetic balance between the divertors, we define $dR_{seq} \equiv (R_L - R_U)$, where R_L is the radius at the outer midplane of the lower divertor separatrix flux surface and R_U is the radius at the outer midplane of the upper divertor separatrix flux surface. Here, we refer to configurations with $|dR_{sep}| \geq 1$ cm as SN, even though the secondary null remains within the vacuum vessel [14].
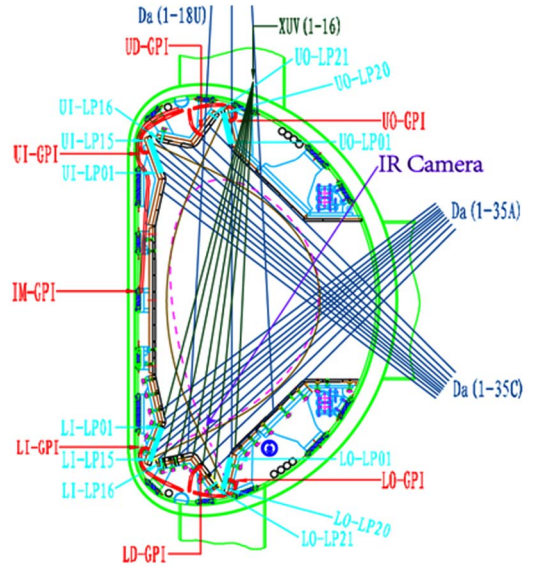
UO(I) - Upper outboard (inboard) divertor, LO(I) - Lower outboard (inboard) divertor, U(L)D - Upper (lower) divertor dome, IM - Inner midplane, LP - Langmuir probe, GPI - Gas puff inlet, RP - Reciprocating probe

Fig.1 Schematic of the EAST cross-section with main divertor diagnostics arrangement and gas puff locations (color online)

EAST has two rather closed divertor chambers [15]. The parameters of the divertor plasma are measured by 74 divertor triple probes embedded in the divertor target tiles, the visible lights with two 35-channel $D\alpha$ radiation arrays viewing the upper-inner and lower-inner target plates and a 18-channel $D\alpha$/CIII radiation array viewing the lower-outer divertor region. The edge parameters in the main plasma are diagnosed by two fast reciprocating probes, two 16-channel extreme ultraviolet (XUV) arrays, and visible light. The electron density is measured by a hydrogen cyanide (HCN) interferometer, while electron temperature is provided by Thomson scattering and heterodyne electron cyclotron emission (ECE) systems, as shown in Fig. 1.

3 Results and discussions

3.1 Radiating plasma behavior in L-modes

The experiments were performed in a balanced DN divertor configuration, with a normal toroidal field, i.e., with the $\mathbf{B} \times \nabla \mathbf{B}$ ion drift toward the lower X-point. The discharges were conducted at $\bar{n}_e \sim 1.5 \times 10^{19}$ m^{-3}, and the Ar mixture gas, i.e., 25% Ar in D$_2$, was injected at 3.5 s at a constant rate for 0.25 s near the outer divertor target strike point

Fig. 2 shows a representative example of DN discharges with the gas mixture (25% Ar in D$_2$) pulse injection, at a constant rate ($\sim 2.6 \times 10^{20}$ particles/s) through the outer target injector. The line-averaged density of the main plasma increases slightly following Ar injection. Both ion saturation current, J_s, and the heat flux at the outer target plate, q_t, are greatly reduced, resulting from Ar injection. This indicates that the outer target enters into the detached plasma regime. Fig. 3 shows the heat fluxes along the target plates before and after the mixed Ar:D$_2$ puffing, obtained from the newly developed divertor IR camera system. As can be seen, the outer divertor target is not only detached on the flux surfaces near the separatrix, but also detached on flux surfaces farther out in the outer leg scrape-off layer (SOL). However, the injected gas was not well confined inside the outer divertor with some leakage into the inner divertor, thus further reducing the particle and heat fluxes to the inner target, accelerating the detachment of the inner leg. Note that the peak particle and heat fluxes at the outer strike point (OSP) are about a factor of 1.5 of those at the inner strike point (ISP) before gas puffing, but after gas injection, the peak particle and heat fluxes at the OSP are significantly reduced, and are even smaller than those at ISP.
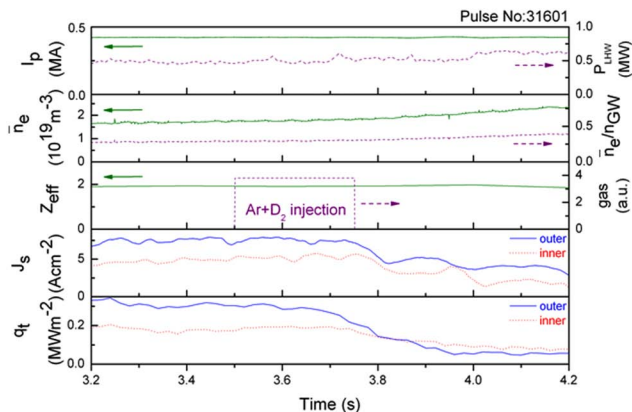

Fig.2 Effect of Ar:D$_2$ mixture gas injection for a typical double null discharge with normal B_T at 3.5 s over 0.25 s (2.6×10^{20} particles/s) from the outer target strike point (Note: the reduction of the heat flux, etc. starts only after the argon puff has been switched off, because the pipeline between the valve and the gas inlet is too long) (color online)
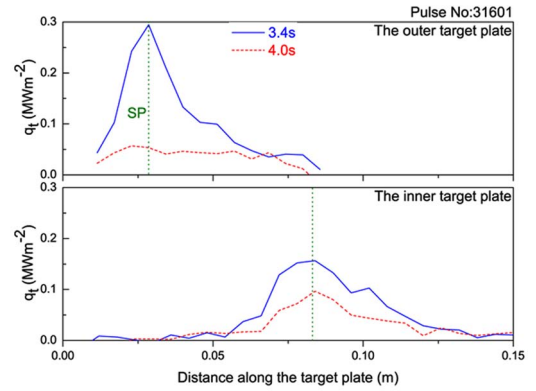
Fig.3 Profiles of heat fluxes at the inner and outer divertor targets which are derived from an IR camera before and after the mixture gas (25% Ar in D$_2$) puffing from the outer target strike points with normal toroidal field in DN (color online)
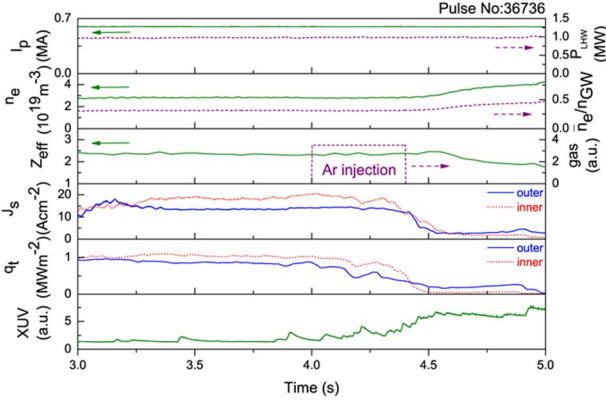
Fig. 4 shows the detailed target profiles of the ion saturation current, J_s, electron temperature, T_{et}, and divertor plasma power flux density, q_t, at the inner and outer divertor targets before and after gas puffing. Clearly, J_s and T_{et} exhibit a pronounced drop at the strike points, leading to a dramatic decrease in the heat flux near the strike points, which is consistent with the IR measurements (Fig. 3).
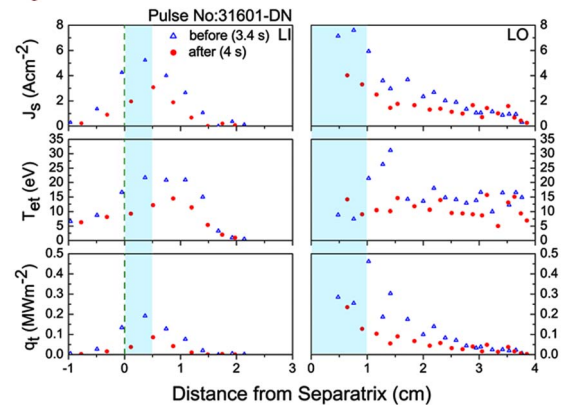
Fig.4 Profiles of ion saturation current, J_s, electron temperature, T_{et}, and power flux, q_t, at the inner and outer divertor targets before and after the mixture gas (25% Ar in D$_2$) puffing from the outer target strike points (color online)

Radiating divertor experiments in SN were also carried out, but with pure argon injection. Argon was injected into the divertor chamber near the OSP, started at $t = 4.0$ s ($\sim 1.26 \times 10^{20}$ particles/s to the lower divertor) over 0.4. As in DN, the argon injection leads to a strong reduction in the particle and peak heat fluxes at both inner and outer divertor targets, as shown in Fig. 5. The reduction in the peak heat flux at the target tiles was primarily due to the increase in radiated power from the X-point/divertor region, accompanied by a sudden formation of a high density, strongly radiating plasma region located between the outer divertor

separatrix strike point and the X-point, as indicated by the measurement from the XUV bolometer. It is remarkable that despite the presence of Ar, the $Z_{\rm eff}$ in the core plasma was actually reduced, presumably due to the increase in the core plasma density after gas puffing.

Fig.5 Effect of Ar injection for a typical single null discharge with normal $B_{\rm T}$ at 4.0 s over 0.4 s (1.26×10^{20} particles/s) from the outer target strike point (Note: the reduction of the heat flux, etc. starts only after the argon puff has been switched off, because the pipeline between the valve and the gas inlet is too long) (color online)

Fig. 6 shows the detailed profiles of the ion saturation current, $j_{\rm s}$, electron temperature, $T_{\rm et}$, and power flux, $q_{\rm t}$, derived from the Langmuir probes at the inner and outer divertor targets before and after Ar injection. Clearly, Ar puffing significantly reduces both particle and heat fluxes, leading to nearly complete detachment at both ISP and OSP. Note that the absolute value of the electron temperature has an error in the later period of the last experimental campaign, i.e., $T_{\rm et}$ is a little higher.
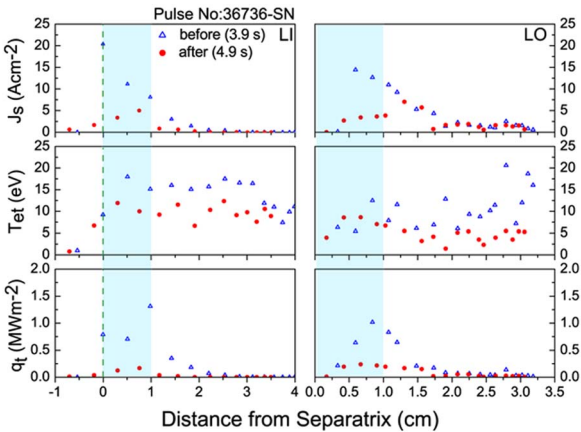
Fig.6 Profiles of ion saturation current, $J_{\rm s}$, electron temperature, $T_{\rm et}$, and power flux density, $q_{\rm t}$, at the inner and outer divertor targets before and after argon gas (pure Ar) puffing from the outer target strike point (color online)

It is interesting to note that both IR and Langmuir probe measurements indicate a stronger divertor asymmetry in the particle and heat fluxes, favoring the outer

divertor in DN than in SN, presumably due to the magnetic geometry with larger heat fluxes to the outer divertor, and enhanced turbulence transport at the outer midplane due to the bad field line curvature in DN [16]. It is also to be noted that the SN discharge (shot 36736) has a much larger total (LHW+Ohmic) input power than the DN case (shot 31601), thus leading to a greater peak heat flux at the divertor target.

3.2 Ar seeding in H-mode

The first H-mode plasma has recently been achieved in EAST with low hybrid wave heating and lithium wall conditioning [17], and impurity seeding into the ELMy H-mode plasmas has been carried out in order to investigate the impurity behavior and to reduce the target heat load in high confinement plasmas. Previous results from JET showed that heavier impurities seem to have a better effect for ELM control while maintaining high density and good confinement [18]. The parameters of the typical ELMy H-mode discharges in EAST are as follows. $I_{\rm P} = 0.6$ MA, $B_{\rm T} = 1.8$ T, $P_{\rm LHW} = 0.9$ MW, $R = 1.85$ m, $a = 0.439$ m, safety factor at the 95% of magnetic flux surface $q_{95} = 3.39$, elongation $k=1.75$ and triangularity $\delta = 0.5$. Pure Ar gas was injected into the lower outer divertor with the SN configuration via the lower outer target injector at 4 s over 0.2 s ($\sim 3.97 \times 10^{20}$ particles/s).

Fig. 7 shows the temporal evolution of some key plasma parameters with Ar seeding. The line-averaged density and plasma stored energy rapidly increases when the plasma enters the H-mode regime at 3.87 s, which is accompanied by some small 'negative' ELMs [19] before transition to type-III ELMs. The intense Ar gas puffing increases the frequency from 0.4 kHz to 0.7 kHz and decreases the amplitude of the
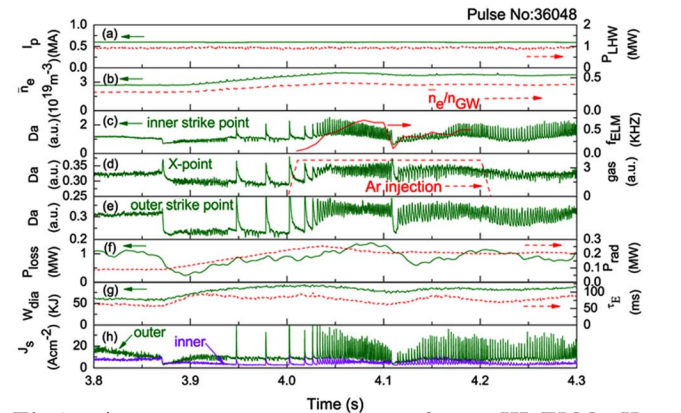
Fig.7 Argon injection into a typical type-III ELMy H-mode plasma: (a) plasma current, low hybrid wave power, (b) electron density, Greenwald density fraction, (c) Dα emission at the inner strike point, ELM frequency, (d) Dα emission at the X-point, Ar puff signal, (e) Dα emission at the outer strike point, (f) loss power, radiation power from the main plasma, (g) energy confinement time, plasma stored energy, (h) ion saturation current of the inner and outer strike points (color online)

type-III ELMs, as indicated by the $D\alpha$ and the ion saturation current, J_s, measured by Langmuir probe at the strike point, followed by a brief transition to the ELM-free phase, at ~ 4.11 s, as seen in Fig. 7(c)$\sim$(e). The detailed physics mechanism of such a transition is unclear and will be further investigated. In particular, both the frequency and amplitude of the ELMs are significantly reduced at the ISP from 4.11 s to 4.16 s after the short ELM-free phase accompanied by radial momentum transport, with the frequency finally settling down to about 0.4 kHz. It is interesting to note that Ar puffing does not appear to significantly affect the plasma stored energy and energy confinement time, with the loss power slightly increased (Fig. 7(f)). The particle and heat fluxes to the divertor target are reduced during the ELMy H-mode, and the particle flux in the H-mode exhibits smaller asymmetry between the inner and outer target than that in the L-mode, as seen in Fig. 7(h).

4 Summary and conclusions

Radiative divertor operation provides an active means to control particle and power fluxes to target plates. The high power, long pulse operation scenarios envisioned for EAST will require impurity seeding to reduce the heat load. A series of L-mode discharges has been carried out in EAST to study radiative divertor plasma behavior in both SN and DN divertor configurations. Argon and its mixture with deuterium (25% Ar in D_2) are injected into the divertor plasmas with active divertor pumping by using a cryopump. As observed in Ohmic discharges [11,12], DN intrinsically exhibits a stronger divertor asymmetry with much larger particle and heat fluxes to the outer divertor target, in contrast to SN. Ar injection leads to a significant reduction in the peak target heat flux for both SN and DN. In particular, the particle and heat fluxes are reduced by a factor of ~ 6 near the outer strike points for DN, thus greatly reducing the in-out asymmetry.

Recently, sustained ELMy H-mode plasmas have been achieved in EAST and argon seeding into the H-mode plasmas has also been investigated. The Ar injection leads to a significant increase in the frequency and decrease in the amplitude of the ELMs. These first results are promising, as a prime motive behind intentional seeding of H-modes with radiating species is to try to lessen intense intermittent particle and heat loads on the divertor target surfaces caused by ELMs, without simultaneously degrading confinement. Controlling ELM energies and resulting surface loads are therefore a key issue for next step devices such as ITER, and will be further explored in EAST for high power, long pulse operations.

References

1 ITER Physics Expert Group on Divertor, et al. 1999, Nucl. Fusion, 39: 2391

2 Petrie T W, Maingi R, Allen S L, et al. 1997, Nucl. Fusion, 37: 643

3 Ingesson L C, Rapp J, Matthews G F. 2003, J. Nucl. Mater., 313$\sim$316: 1173

4 Fenstermacher M E, Boedo J, Isler R C, et al. 1999, Plasma Phys. Control. Fusion, 41: A345

5 Kallenbach A, Dux R, Fuchs J C, et al. 2010, Plasma Phys. Control. Fusion, 52: 055002

6 Takenaga H, Kubo H, Higashijima S, et al. 2002, Fusion Science and Technology, 42: 327

7 Lipschultz B, Labombard B, Terry J L, et al. 2007, Fusion Science and Technology, 51: 369

8 Yan L W, Hong W Y, Cheng J, et al. 2009, J. Nucl. Mater., 390$\sim$391: 246

9 Wan Yuanxi, HT-7 Team, HT-7U Team. 2000, Nucl. Fusion, 40: 1057

10 Weng P D, Chen Z M, Wu Y, et al. 2005, Fusion Eng. Des., 75$\sim$79: 143

11 Guo H Y, Gao X, Li J, et al. 2011, J. Nucl. Mater., 415: S369

12 Wang Dongsheng, Guo Houyang, Wang Huiqian, et al. 2011, Phys. Plasmas, 18: 032505

13 Petrie T W, Brooks N H, Fenstermacher M E, et al. 2008, Nucl. Fusion, 48: 045010

14 Petrie T W, Porter G D, Brooks N H, et al. 2009, Nucl. Fusion, 49: 065013

15 Wang Dongsheng, Li Qiang, Xu Qian, et al. 2010, Fusion Eng. Des., 85: 1777

16 Stangeby P C. 2000, The Plasma Boundary of Magnetic Fusion Devices. IOP Bristol

17 Xu G S, Wan B N, Li J G, et al. 2011, Nucl. Fusion, 51: 072001

18 Maddison G P, Brix M, Budny R, et al. 2003, Nucl. Fusion, 43: 49

19 Loarte A, Monk R D, Martín-Solís J R, et al. 1998, Nucl. Fusion, 38: 331